Abraham Kribus[1]
e-mail: kribus@eng.tau.ac.il
Dept. of Fluid Mechanics and Heat Transfer
Faculty of Engineering,
Tel Aviv University,
Tel Aviv 69978, Israel

Irina Vishnevetsky

Moshe Meri

Amnon Yogev

Environmental Sciences and Energy Research,
Weizmann Institute of Science,
Rehovot 76100, Israel

Andrei Sytnik
Falcon Technologies,
P.O. Box 57185,
Tel Aviv 61571, Israel

Continuous Tracking of Heliostats

Tracking motions in current heliostats are usually performed in discrete steps, even though the motion of the sun is continuous. Aiming errors due to the discrete steps are often about 1 mrad or more. A significant reduction of tracking error by smooth continuous tracking is presented. The implementation uses an electronic speed control unit to modify the rotational speed of the two AC motors on an existing heliostat. The continuous tracking system was implemented and successfully operated at the Weizmann Institute heliostat field. Measurements of heliostat motion show that aiming error due to tracking intervals was practically eliminated. A comparison of heliostat motions and flux on the target in step-tracking and continuous tracking modes is reported.
[DOI: 10.1115/1.1668026]

1 Introduction

Many modern solar energy conversion processes require elevated temperatures, often above 1000°C. High concentration of sunlight is needed for efficient operation of these high-temperature processes, often significantly above 1000 suns. Current technology of heliostat fields is usually used to produce average concentration ratios of up to 1000, although higher concentration is theoretically possible [1]. The performance of heliostat fields is limited by geometric errors in the heliostat structure (surface errors) and in its operation accuracy (tracking errors). The heliostat errors reduce the concentration potential since they effectively spread the reflected radiation over a wider angular range than the original solar disk. Secondary concentrators are commonly used to boost the concentration when the heliostat field cannot provide the required levels [2–4]. This involves additional expense and additional power losses. In addition, secondary concentrators cannot recover the lost thermodynamic potential due to heliostat errors. It would be therefore beneficial to improve the performance of the heliostat field, reducing the need for secondary concentration whenever possible. One of the heliostat error sources, the tracking error, is addressed in the current work.

The common errors in heliostat tracking control are usually about 1–1.5 mrad, and can be more in some situations [5–7]. These errors are due to many factors, such as: drive tolerances and backlash; accuracy of the sun's position model; interval between heliostat motions (due to encoder resolution); structure deformation due to gravity and wind. The influence of these factors can have very different time scales. Errors such as sun's position model inaccuracy and drift due to gravity bending occur on a relatively long time scale. A possible solution to detect and eliminate these errors is a closed-loop control system [8]. However, errors generated by the intermittent motion of the heliostat motors have a relatively short time scale, and may not be detected effectively by the closed loop.

In most of the current heliostat tracking designs, the heliostat remains stationary until sufficient angular error has accumulated due to the motion of the sun, and then corrects the error in a relatively rapid motion stroke. The drift of the image between corrections can be significant; for example, at the WIS heliostat field a typical drift of 20–30 cm on the target plane has been measured, corresponding to an aiming error of about 1 mrad. This is significant relative to the size of the solar disk half-angle, which is about 4.65 mrad. This drift therefore causes a significant reduction in the time-averaged flux concentration incident on a receiver. In addition, the rapid correction motion can induce vibrations in the heliostat structure that cause the sun's image to oscillate around the target for several seconds. These oscillations also lower the time-averaged flux concentration.

These problems can be practically eliminated when the heliostat motors operate continuously at a low and variable speed, to match the apparent motion of the sun. In principle, it should be possible to eliminate tracking errors completely using the combination of continuous motion (to eliminate short time scale errors) and closed loop control (to correct longer time scale errors). This would reduce considerably the overall heliostat error, and can improve significantly the capability of heliostat fields to reach higher concentration.

As a rough estimate of the significance of tracking error, consider the effect of the error on the thermodynamic limit of concentration of solar radiation. The half-angle of the solar disk on a clear day is $\theta_s = 4.65$ mrad, leading to a maximum theoretical concentration ratio of: $C_{\max} = 1/\sin^2 \theta_s = 46{,}000$. If the time-averaged angular tracking error increases the effective solar disk (''degraded sun'') to 5 mrad, then the maximum theoretical concentration is reduced to about 40,000. This is a 13% reduction in the concentration potential, and can reduce the intercepted power and the efficiency of high-temperature receivers operating under highly concentrated radiation. Eliminating the tracking error by the use of continuous tracking can recover this lost potential.

The possibility of continuous tracking using stepper motors or DC motors is well known, but not very popular in industrial designs. One reason can be the relative high cost of stepper and DC motor drives, compared to AC motors. The only well-documented attempt to use continuous tracking included a heliostat in a solar furnace [9]. They have developed servo-unit based electronics to drive the heliostat DC motors at the required low speeds. Experimental measurement of the power drawn by the motors was re-

[1]Corresponding author: tel. +972-3-6405924, fax +972-3-6407334
Contributed by the Solar Energy Division of THE AMERICAN SOCIETY OF MECHANICAL ENGINEERS for publication in the ASME JOURNAL OF SOLAR ENERGY ENGINEERING. Manuscript received by the ASME Solar Energy Division, May 2003, accepted as is. Associate Editor: J. Davidson.

ported, but not the effect of the tracking on the power and flux distribution at the target. Such an implementation cannot be used in common heliostat designs that employ AC motors, without considerable redesign.

We present an implementation of continuous tracking system that can be applied to existing heliostats and existing heliostat designs with a minimum of changes. The continuous tracking system was developed and implemented on a heliostat at the Weizmann Institute of Science (WIS) solar field. Test results are reported, and significance to future heliostat fields is discussed.

2 Analysis

2.1 Tracking Speed Requirements. The required speeds for the heliostat motors, in order to track accurately the motion of the sun, can be derived from the sun's direction vector data [10]. For example, consider the conditions typical for the Weizmann Institute field at 32° latitude, a heliostat with azimuth-elevation drive located one tower-length (50 m) north of the tower, and the same gear ratio as in the WIS heliostats (41,202). The required tracking motor speeds in both axes are shown in Fig. 1. Providing motors rotating at variable speed down to 15 RPM, for example, will enable continuous azimuth tracking through much of the time except near winter solstice. This speed, however, is not low enough for the elevation drive. A motor with speed adjustable down to 5 RPM, however, will provide continuous azimuth tracking throughout the year, and continuous elevation tracking most of the time, except near noon.

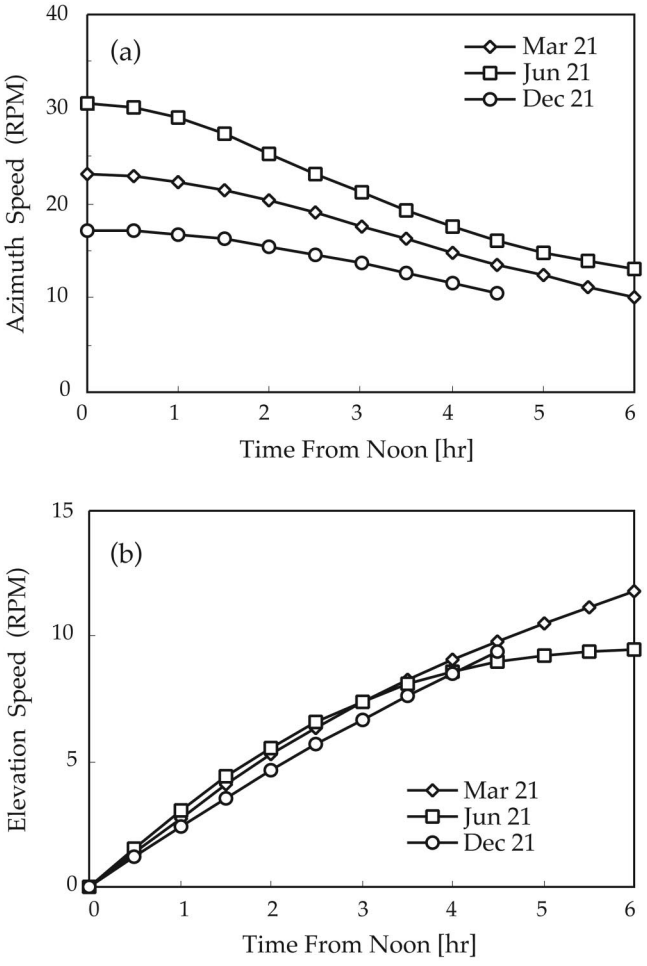

Fig. 1 Heliostat motor speed requirements for continuous tracking: (*a*) azimuth, (*b*) elevation.

2.2 Effect of Aiming Error. The WIS heliostats contain two encoders of 8192 (2^{13}) counts per shaft revolution to determine the angular position in the two rotation axes. The interval between encoder bits is the smallest step that the existing heliostat control can detect. The smallest angular motion of the sun that can be tracked is twice the minimal angular step of the heliostat, i.e., 1.53 mrad. This increment in the angular position of the sun takes about 21 seconds. For a heliostat with slant range of 60 m, the aiming error on the target at the end of this interval is 0.09 m. The aiming error varies linearly with the slant range.

The possible reduction in collected power due to drift error was estimated for a heliostat with slant range of 60 m. Ray tracing was used to compute the flux distribution on the target, assuming that the sun's position is behind the target (on-axis) so the image projected on the target is circular and relatively free of aberrations. A circular aperture of radius 0.25 m collects about 90% of the incident radiation (Fig. 2). The flux distribution was moved relative to the aperture, representing the aiming error, and the change in intercepted radiation was computed. The intercepted power decreases with increasing drift error, up to 16% for the maximum expected drift of 1.5 mrad, as shown in curve I of Fig. 2(*b*). The time averaged loss is about 8%, assuming that the drift increases linearly with time.

In the case of a partitioned receiver system [11,12], the total aperture is divided into several smaller apertures corresponding to separate receiver units. Partitioned systems usually need polygo-

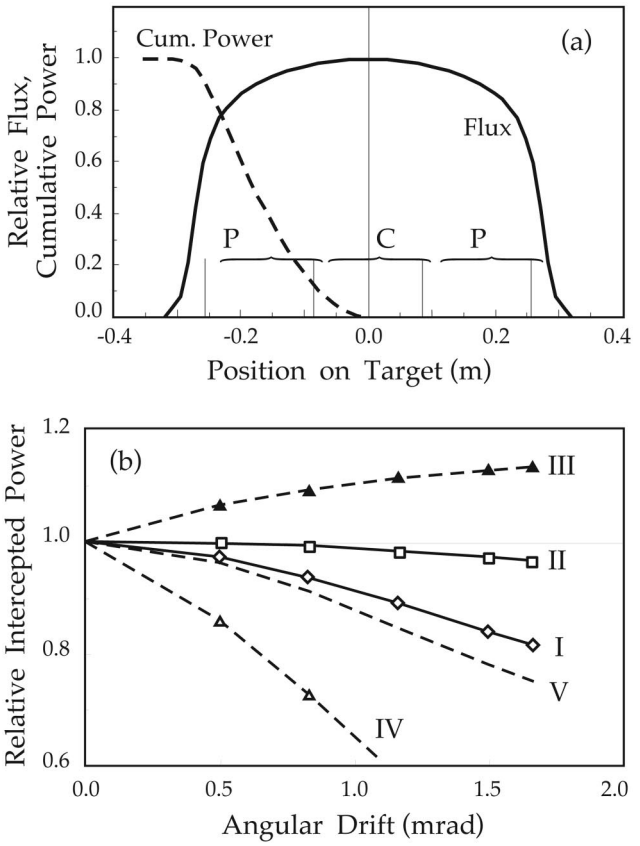

Fig. 2 (*a*) Flux distribution and cumulative power on the target. C and P indicate the apertures of the central and peripheral units in a partitioned receiver, respectively. (*b*) Variation of the intercepted power by each aperture as a function of aiming error: a single large receiver (I), the central unit in a partitioned receiver (II), a peripheral unit in a partitioned receiver when the aim point drifts closer (III), a peripheral unit when the aim point drifts away (IV), the average of two opposite peripheral units (V).

Table 1 Measurements of heliostat image drift and bounce in the existing step control method.

Hel. No.	Slant Range (m)	Start Time	End Time	Drift (m)	Bounce (m)	Avg. Step (s)
100	67	09:58	10:05	—	0.1-0.2	20.5
302	85.5	10:32	10:38	0.2-0.3	—	20.4
500	111	10:20	10:30	0.2-0.3	0.3	20.8
602	127.5	09:47	09:57	0.2-0.4	0.1-0.3	21.8

nal apertures, not necessarily of the same size. However, the current estimate assumes circular units of equal 0.17 m diameter, to preserve the simplicity of the computation. The division of the aperture into a central unit surrounded by peripheral units is shown in Fig. 2(*a*). The power intercepted in the central unit varies only by 3% at the maximum drift of 1.5 mrad, as shown in curve II of Fig. 2(*b*), since the gradient of the incident flux distribution is small near the center.

A peripheral unit, on the other hand, experiences strong variations: up to 13% increases as the aim point drifts towards it (curve III), and up to 56% decrease as the aim point drifts away from it (IV). The decrease in case IV is especially prominent, since drift of the aim point away from this unit brings the sharp gradient of the flux distribution into the aperture. The average of two peripheral units located on opposite sides of the target (V) is also strongly decreasing, up to 22% at maximum drift, since the decrease in IV is faster than the increase in III. The overall effect of aim point drift on a partitioned receiver system is therefore not only an overall decrease in intercepted power, but also variations in the balancing of the different receiver units. The peripheral units need to be designed to tolerate higher power than their average rating, and the receiver control system needs to allow large-amplitude variations in power of individual units. Alternatively, the thermal capacitance of each unit should be high enough to absorb and smooth these oscillations.

The estimates presented above refer to a single heliostat under ideal conditions. In a full heliostat field, where the flux distribution is produced as an overlap of many heliostats, the variations due to aim point drift will be smaller. Nevertheless, when the application requires high flux and high efficiency, the loss due to aiming errors can be significant.

3 Tracking System

3.1 Existing Step Tracking System. Each heliostat at the WIS field has two AC motors with constant 1350 RPM speed, each with a reduction gearbox with ratio of 41,202. An encoder attached to each axis measures gear exit shaft position and transmits it to the Heliostat Control (HC). A central field computer calculates the required position (azimuth and elevation) for each heliostat every half-second. This information is transmitted through fiber optic lines to the HC. The HC compares the requirement with the encoder position reading. If the difference is greater than one encoder count unit, a correction command is created. The encoder minimal step corresponds to approximately five turns of the motor shaft. The rotation is performed in short bursts: the motor receives a series of 20 millisecond pulses that each creates approximately 2.5 turns. This tracking algorithm, often called 'bang-bang' control, has two effects. One is a drift of sun's image on the target plane away from the aim-point, with intervals of 20 seconds or more between corrections. The interval is determined by the encoder resolution. The second effect is a 'bouncing' oscillatory movement lasting several seconds after each tracking motion, caused by the sudden acceleration and deceleration.

The drift and bounce errors were measured for four heliostats at different positions in the field by video photographing the heliostats' sun images on a target surface. The images were projected on the north wall of the Solar Tower. Linear measurements were estimated by comparison to the Tower wall tiles, with a possible measurement error of ± 0.1 m. The measurement results are shown in Table 1. The average time interval between heliostat position corrections was 21.1 s. The drift was in the range of 0.2–0.4 m, and the bounce amplitude was in the range of 0.1–0.3 m.

The nominal tracking error of the heliostat, as stated by the manufacturer, is 2.04 mrad RMS. The angular error based on the measured drift is about 2–4 mrad near the end of the tracking interval, and a time averaged drift error would therefore be about 1–2 mrad. The instantaneous contribution of the bounce error can reach 3 mrad, but this error exists for about 5 seconds out of a typical interval of 20 second, and therefore its time-averaged contribution should be up to 0.75 mrad. Overall, it seems that the actual aiming errors are consistent with the nominal value.

3.2 Hardware Implementation. The continuous tracking system was installed in heliostat 307 at the WIS field. It was implemented using Electronic Speed Controllers (ESC) added to the existing AC motors. Two speed controllers model SB1091BE (ACS Electronics Ltd., Israel) were used. This controller contains a digital AC servo motion control module, designed to control any type of three-phase motor. It uses a field oriented control technique (flux vector control) where position, velocity and motor current are simultaneously monitored to provide optimal operating conditions. The current loops, the velocity loop, position loop, and the commutation are implemented by software with a 200 kHz sampling rate. The three motor leads can be connected in an arbitrary way, and the controller identifies the connection and determines autonomously how to drive the motor. The controller can be operated in different motion-control modes, such as: position, velocity, manual joystick, master/slave follower, etc.

The heliostat motors were modified to permit operation with the speed controller. The fan installed in the motor back was removed, and an encoder was installed on the back shaft (Fig. 3). The encoder was installed on a back plate that is spaced from the motor by extension rods. Coupling to the shaft is accomplished via a

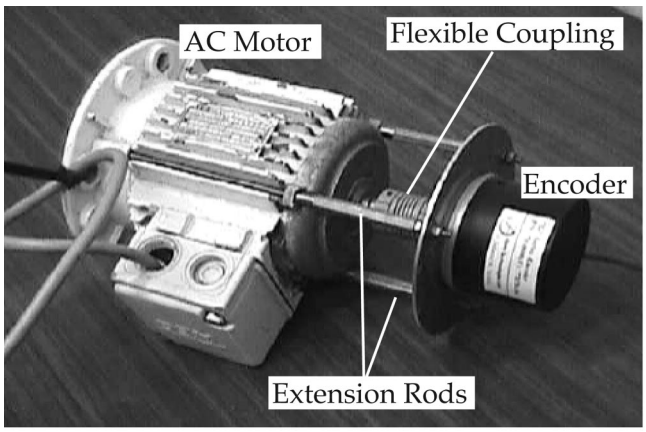

Fig. 3 Modified heliostat motor with an external encoder mounted on the back shaft.

flexible coupler (Helical model ASM-100) that compensates for any misalignment. This encoder features 4096 counts per revolution of the motor. This provides very precise information about the heliostat position, since mechanical backslash is negligible.

The modified heliostat control was implemented independently of the field's central control system, to permit the rest of the field to operate normally with the existing central control. The existing Heliostat Controller (HC) unit was disabled and replaced with a stand-alone PC. The PC provided both the operator interface (replacing the central field control) and supervision of the speed controllers (replacing the HC). Communication with the ESC was via a RS-422 cable. In a commercial scale solution, a single PC can control many ESC units in different heliostats, and provide the operator interface for all heliostats at the control room. The use of RS-422 communications standard permits a distance of up to 1 km between the heliostat and the control room, which is more than adequate.

3.3 Software Implementation. The continuous tracking algorithm proceeds as follows:

- Read the current angular position of the heliostat from the motor encoder
- Compute the required heliostat position from astronomical correlation
- Compute the angular position error: the difference between required and current position
- Compute a speed correction based on the angular position error
- Generate a speed correction command.

The speed correction ΔV (measured in motor encoder bits per second) is:

$$\Delta V = -\frac{\Delta\alpha N_E G}{360}\cdot\frac{1}{C} \tag{1}$$

$\Delta\alpha$ is the angular position error (degrees), $N_E = 4096$ is the motor encoder bit count per revolution, and $G = 41202.43$ is the gear reduction ratio. C is an empirical feedback factor; a value of $C = 7$ was usually best for smooth operation without overshoot.

The tracking loop was repeated approximately every 0.7 seconds. This high rate is not really necessary; in velocity controlled motion, accumulating an aiming error of 0.1 mrad can take several minutes [9]. It is therefore possible to control a large number of heliostats with a single PC while keeping the errors at negligible values.

Operator interface software was developed in Visual Basic on the PC. Control over the ESC is established via a proprietary library of subroutines supplied by ACS. The controller commands are downloaded and saved in the controller, and therefore communication between the controller and the PC is needed only to specify changes in the tracking. The heliostat control software provides three operation modes: continuous motion of the heliostat following the apparent motion of the sun; administrative motions (to Stow, Standby, etc.) at full motor speed; and emulation of the old 'bang-bang' tracking method to enable performance comparisons. The emulation is possible since the gear has negligible backlash, providing good correspondence of input and output shafts; and since the resolution of the new encoder is high enough to represent a correction step, on a time scale much shorter than the old encoder tracking interval. The operator can easily switch between the different modes during system operation. The software also accepts external aiming corrections that are made either manually by the operator, or automatically from external sources such as a closed-loop control system [8].

3.4 Test Platform. The test target was installed at the Solar Tower's ninth floor (Fig. 4). The target consists of a square 2 $\times$2 m surface made of alumina boards. A small aperture (0.08 m^2) at the center of the target leads to a small secondary concentrator and a calorimeter. The concentrator and calorimeter were constructed for a previous project [13], and serve here to measure the average flux incident at the center of the target. The secondary concentrator is constructed from planar back-silvered glass reflectors glued to water-cooled aluminum plates. The calorimeter is a cylindrical cavity fabricated from copper sheets, painted black on the inside, and water-cooled by copper tubes attached to the outside surface by a high-conductivity adhesive. The water inlet and outlet temperatures are measured by J-type thermocouples. A manual Float Rotameter model KSK (Manoraz, Israel) measures the water flow rate.

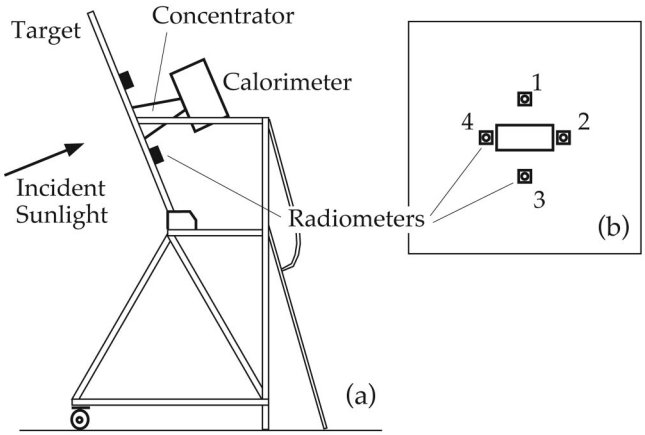

Fig. 4 Target and test platform: (*a*) side view, (*b*) front view of the target.

Four radiometers model 150W-BNC-Y (Ophir, Israel) were installed around the center of the target. They measure the incident flux at a radius of 0.5 m around the center of the target. This position of the radiometers represents the conditions near the periphery of a typical receiver aperture.

The data acquisition system includes two Advantech ADAM-4018 analog input modules. The two modules are daisy-chained by an RS-485 communication line to a Pentium 166 PC. The input modules read, amplify and translate the signals to engineering units according to software settings. GENIE software running on the PC displays the readings and saves the data to disk. Communication between the test PC and the heliostat control PC was provided by an RS-422 connection and two ADAM-4520 communication adapters.

4 Continuous Tracking Tests

Seven test days were accomplished with alternating continuous and step tracking modes. The main objective of these tests was to compare the new continuous tracking mode to the previous step tracking, which was produced by the simulation mode in the new control software. The tests were performed during a period when the incidence angle on the heliostat was about 10–15°. The off-axis aberration was therefore relatively small, and the effects of the tracking error were not masked by a large and varying aberration.

4.1 Heliostat Motion. The heliostat angular position (elevation and azimuth axes) is known with high accuracy due to the new motor encoder, which offers much higher resolution than the old heliostat encoder does. The heliostat gear backlash is negligible, and therefore the new encoder installed on the motor shaft can be considered accurate. The heliostat position during a typical period of alternating step and continuous tracking are compared in Fig. 5. In the step-tracking mode, the discrete increments of angle are seen in both axes. The angular size of the step is the same in both axes, corresponding to the minimal rotation that can be detected by the heliostat encoder (0.044°, 0.77 mrad). The time was

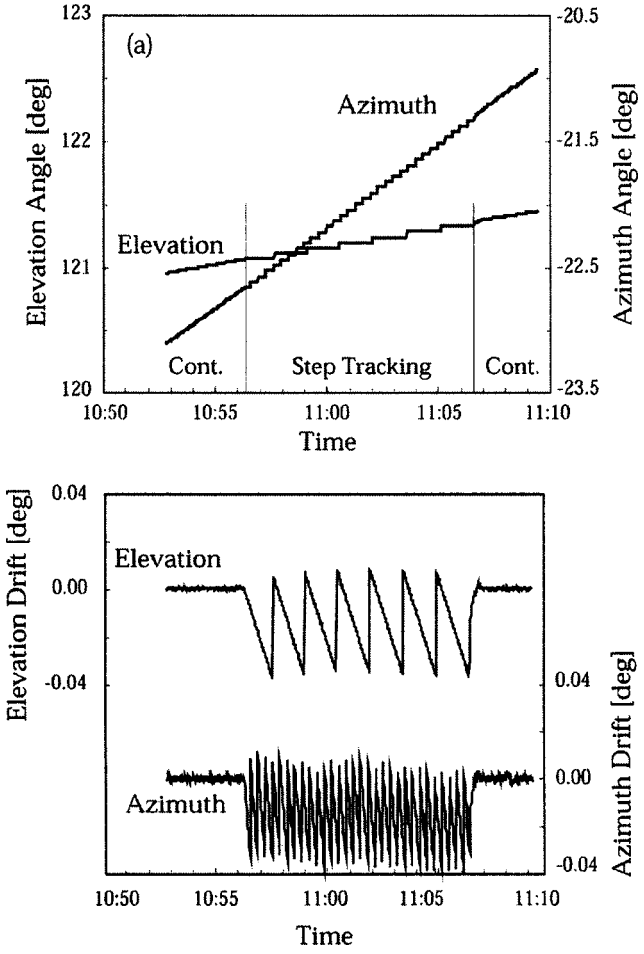

Fig. 5 (*a*) Variation of elevation and azimuth angles of the heliostat during continuous and step tracking. (*b*) Drift of the heliostat angles from the exact aiming.

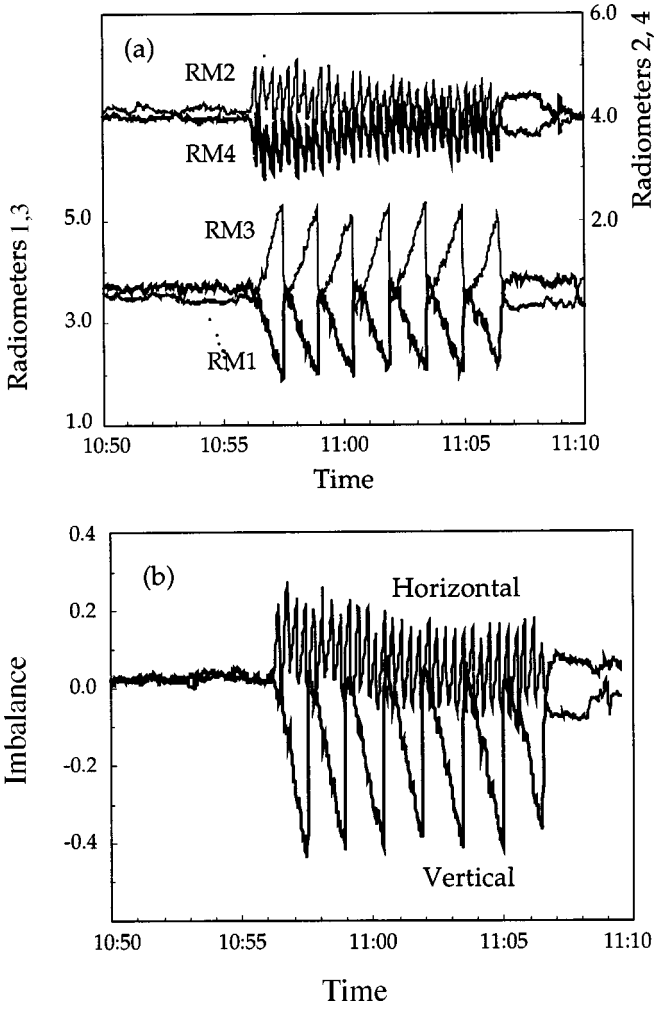

Fig. 6 Variation of the radiometer measurements during periods of continuous and step tracking: (*a*) individual radiometers, (*b*) imbalance.

near noon and therefore the rate of change in azimuth was faster than the elevation. The continuous tracking mode shows smooth variation of both angles.

The deviation of the actual angular position from the exact aiming, i.e., the drift error, is shown in Fig. 5(*b*). The amplitude of the drift error in step tracking mode corresponds to the heliostat encoder step size. The error is mostly negative for both the azimuth and elevation axes, since the correction is lagging behind the motion of the sun. This indicates that the error induced by the step motion is consistent in one direction rather that distributed randomly about the correct aiming value. The maximum angular error in either axis is about 0.7 mrad, corresponding to 1.4 mrad error in the direction of the reflected radiation. This would cause a displacement of 0.11 m on the target plane if the distance to the target is 80 m and the target is perpendicular to the incident radiation. The displacement on the target will be higher for a more distant heliostat and for a heliostat located away from the normal to the target.

The aiming errors that occur during step tracking are very visible when considering the power measured by the radiometers, Fig. 6(*a*). The measurements are very stable during the continuous tracking periods, while the measurements during the step tracking period show regular oscillations. The amplitude of the oscillation is larger in the vertical direction than in the horizontal direction. The instantaneous change in measured flux can reach 50% in the vertical radiometers, indicating that the small aiming errors during step tracking can create large oscillation in incident flux at the periphery of the target. The relative change in the horizontal direction is smaller, but can reach 25%, which is also significant. The difference between the two directions is probably due to the asymmetric flux distribution rather than a difference in the directional error, since the maximum angular error is the same in both tracking axes, as seen in Fig. 5.

The effects of aim point drift can be characterized by a comparison of the flux on two opposite sides of the aperture, Fig. 6(*b*). We defined an imbalance $IMB_{M\text{-}N}$ for each pair of opposite radiometers *M, N* from the measurements RM_M, RM_N:

$$IMB_{1-3} = ln\left(\frac{RM_1}{RM_3}\right)$$

$$IMB_{2-4} = ln\left(\frac{RM_2}{RM_4}\right) \tag{2}$$

Both imbalances are very small during the continuous tracking period. When step tracking starts, the individual radiometer readings and both imbalance signals become oscillatory. The vertical imbalance is mostly negative, since the motion of the sun is in the upward direction (time is before solar noon) and the heliostat lags behind this motion. The radiation is therefore reflected lower than the aim point. This leads to an increase in the lower radiometer (No. 3) and a decrease in the upper radiometer (No. 1), producing a negative imbalance. The horizontal imbalance tends to be positive since the motion of the sun is towards the West, producing a drift of the radiation to the East when the heliostat remains sta-

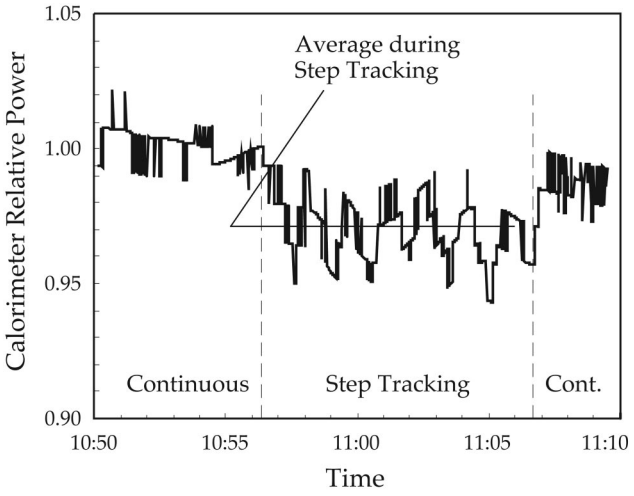

Fig. 7 Relative power collected by calorimeter. Vertical lines: beginning and end of step tracking.

tionary. This creates an increase in the East radiometer (No. 2) and reduces the West radiometer (No. 4), leading to a positive imbalance.

4.2 Power on Target. The power incident on the central calorimeter during periods of continuous and step tracking is shown in Fig. 7. Observation of the data revealed that the calorimeter power variations lagged the changes in insolation by about two minutes. Due to the high thermal capacitance of the calorimeter, the power extracted at a given time is an integral of the power absorbed in the receiver during the previous few minutes. The collected power was therefore adjusted relative to the average insolation during the two minutes preceding the measurement.

A decrease in the calorimeter power is seen at the onset of step tracking. The power is oscillatory during this period, compared to more stable behavior during the preceding and following continuous tracking periods. The largest decrease in power during the period of step tracking was about 6% relative to the average collected power during the preceding continuous tracking period. The time-averaged power loss during step tracking was about 3%. The predicted time-averaged decrease corresponding to a central unit in a partitioned receiver system (curve II, Fig. 2) was 1.2%. The larger power loss measured in the experiment probably indicates that contrary to the computational model, the actual flux distribution was not flat at the center of the target. The effects of heliostat surface and canting errors caused the distribution to be more peaked at the center, leading to larger power loss as the center of the distribution moves away from the center of the aperture.

The behavior of the flux at the periphery of the target during step tracking was considered next. Both elevation and azimuth steps that occur during normal tracking affect the flux measured by each radiometer. In order to separate the effects of the two orthogonal corrections, the data was filtered as follows: the elevation error and the measurements of the vertical radiometer pair (1 and 3) were selected at times when the azimuth error was close to zero, i.e., immediately following an azimuth correction. The dependence of radiometer reading on the elevation error is shown in Fig. 8(*a*). The largest differences in the local flux are around 40% relative to the centered (no aiming error) position. Also shown are curves III and IV from Fig. 2, representing the predicted effect of the error on two peripheral apertures on opposite sides of the target center, similar to the location of the radiometers. The prediction is good for radiometer 1, while the variation of radiometer 3 is much higher than the prediction. The reason could be again a deviation of the flux distribution from the model used in the prediction.

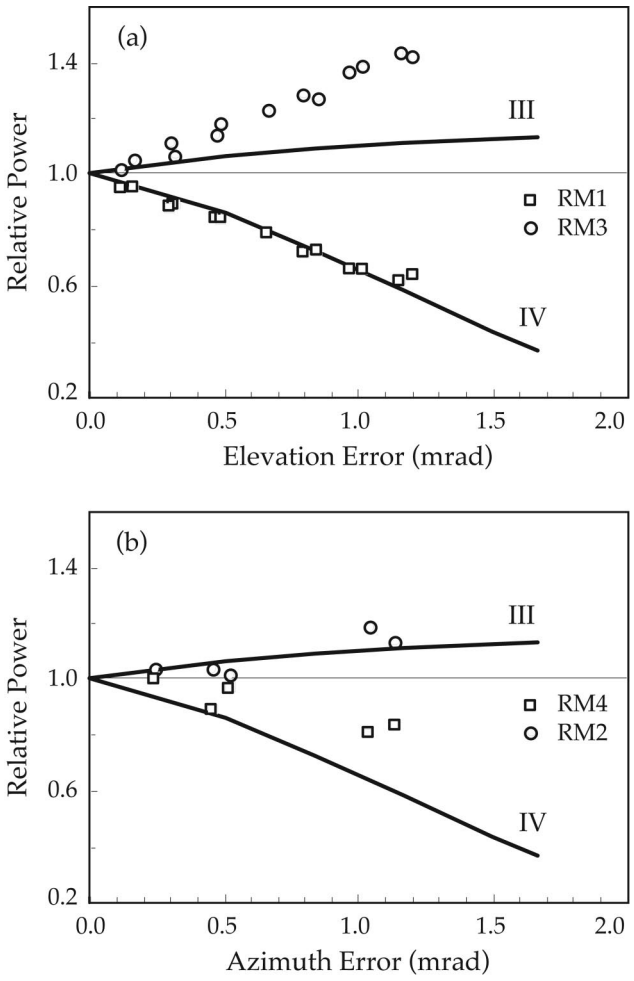

Fig. 8 Variation of flux measured by the radiometers as a function of (*a*) elevation error, (*b*) azimuth error.

A similar analysis isolates the azimuth error and horizontal radiometer pair at times when the elevation error is close to zero, immediately following an elevation correction step. The results are shown in Fig. 8(*b*). The results for radiometer 2 are similar to the prediction, while radiometer 4 has the same trend but different values. The largest variations in the local flux are around 20% relative to the centered (no aiming error) position.

The comparison shown in Fig. 8 is not expected to show exact correspondence, since the radiometers are point measurements while the prediction referred to large apertures. In addition, the decoupling into azimuth and elevation errors does not correspond exactly to horizontal and vertical aiming errors on the target. The flux distribution on the target was also different from the simple distribution used in the model, both due to heliostat geometric errors as mentioned above, and due to astigmatic aberration that produces a non-circular distribution. Therefore, only qualitative correspondence was expected.

4.3 Oscillations. The strong link between the variations in measured power and the tracking motions can be observed in a spectral analysis. A Fourier transform was applied to sets of 512 data points each, corresponding to periods of 511 seconds (about 9 minutes). The absolute magnitude of the Fourier modes indicates the energy content of each frequency. Figure 9 shows the resulting spectra for the calorimeter power and for radiometers 1 and 2, comparing the continuous and step tracking periods. The calorimeter and radiometer 1 measurements during step tracking show a strong peak at a frequency of 0.0117, corresponding to a period of

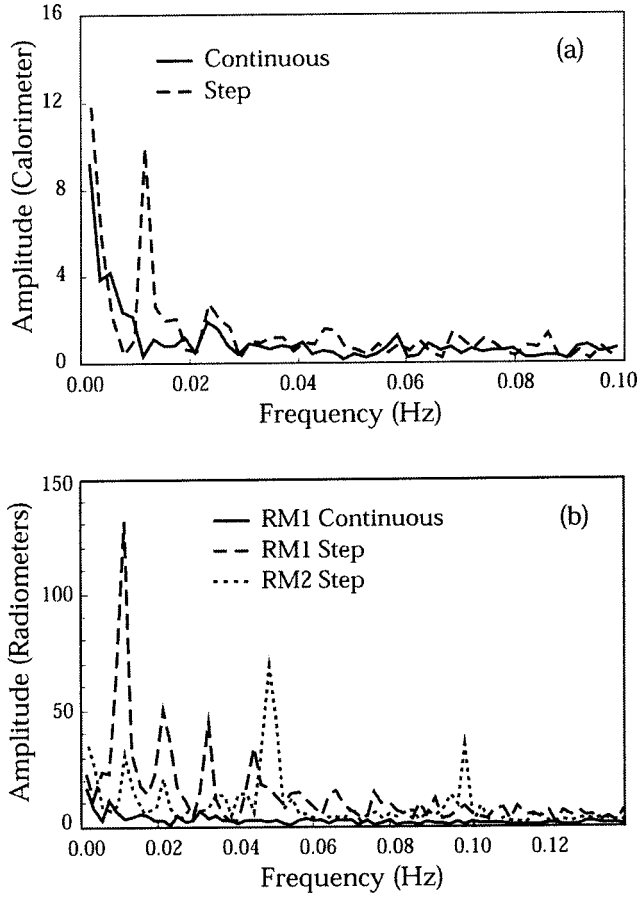

Fig. 9 Spectra of (*a*) calorimeter power, and (*b*) radiometer 1 and 2 measurement.

85 seconds. This matches the frequency of steps in the elevation axis of the heliostat, as seen in Fig. 5. This peak is absent in the corresponding continuous tracking spectra. Radiometer 2 shows a smaller peak at this frequency, since the effect of elevation corrections is stronger for the vertical pair (1,3) than for the horizontal pair (2,4).

Wind during the test was very low, and apparently any structural vibrations due to wind loads were negligible. The spectra presented here do not seem to show any significant peaks that are not related to the proper tracking motion.

A large peak is present in the spectrum of radiometer 2 for step tracking at a frequency of 0.0488, corresponding to a period of about 20 seconds. This matches the frequency of tracking steps in the azimuth axis of the heliostat. A peak at the same frequency is present also in the calorimeter and radiometer 1 spectra for step tracking. The calorimeter peak is much smaller, due to its high thermal capacitance, which attenuates higher frequency fluctuations. The peak for radiometer 1 is also small since the vertical pair is less sensitive to azimuth corrections. This frequency is absent from the continuous tracking spectra.

Additional significant peaks are present for step tracking of radiometer 1 at frequencies of 0.0215 to 0.0332, corresponding to periods of about 30 and 46 seconds. These are probably higher harmonics of the primary elevation correction frequency, and are present since the correction is performed in an abrupt step rather than as a pure Fourier mode. A peak at frequency 0.0966 (10 seconds period) in the spectrum of radiometer 2 is also a harmonic of the primary 20 seconds period. At higher frequencies, all spectra are relatively small.

5 Discussion

Continuous tracking of a heliostat was implemented using a new control system that replaced the existing heliostat controller electronics, but retained the existing heliostat motors. The new system included two Electronic Speed Controllers installed at the heliostat, and a remote PC that in principle can drive many heliostats. Testing of the new control system has shown that smooth heliostat motion can be achieved down to the lowest required tracking speed, and that tracking error due to intermittent heliostat motion can be reduced to negligible levels. The differences between step tracking and continuous tracking were clearly observed during the tests. The motion of the heliostat motors during continuous tracking was smooth and uniform. The motions in step tracking were characterized by oscillation with two distinct frequencies, corresponding to the azimuth and elevation correction intervals.

The effect of switching the control method was clearly felt by sensors located at the center and at peripheral radial positions on the target. During continuous tracking, the power measurements and the radiometer imbalance were relatively stable with some 'noise' about the average value. During step tracking, the power and radiometer imbalance showed some reduction and large oscillations. The oscillations were well correlated with the frequency of the heliostat aiming corrections. The time-averaged measured gain in the flux near the center of the target was 3% in continuous tracking compared to step tracking. The differences in flux at the peripheral positions between the two tracking modes were up to 40%. The continuous tracking mode provided therefore higher power (higher intercept efficiency) and much more stable flux distribution on the receiver.

These point measurements are encouraging indicators, but not sufficient as a representation of a real receiver. Testing with a full receiver is needed to evaluate the gain in average power. According to the model prediction presented above, a typical receiver may gain about 8% more power when switching from step to continuous tracking; this should be validated under real field conditions. Another aspect that needs further analysis is the extension of the continuous tracking solution from a single heliostat to a full heliostat field. This type of analysis will provide information about the effect of correcting the tracking error relative to other issues such as astigmatic spread. The relative significance of this correction relative to other factors affecting field performance can then be derived. This analysis should be performed before further investment in developing the continuous tracking system.

The continuous motion system can provide other benefits, in addition to increased average power into the receiver. Motor heating was significantly reduced, and the motors were cooler even though the standard cooling fan was removed. The abrupt acceleration and strong inertial forces that load the motors, gear and structure during start-stop transients were eliminated. These features can lead to higher reliability and longer equipment life. The increased accuracy of the motor encoder can save the need for the high-resolution expensive heliostat-side encoder, especially if closed loop aiming corrections are also employed.

Aiming error due to step tracking is only one cause of degradation in heliostat field performance. Other possible sources are related to, for example, the heliostat construction and alignment accuracy, gear backlash, or deformation due to wind pressure. Eliminating one type of error by continuous tracking does not, obviously, eliminate other sources of error. Each heliostat design should be characterized to analyze in detail the different error sources, and the relative significance of each source. A high-performance heliostat field should then employ a balanced set of techniques for error reduction, considering the cost of each error correction measure vs. its contribution to the overall performance improvement.

Closed loop dynamic aiming correction [8] is an attractive technique for high-performance heliostat fields. Use of step tracking in this case will introduce significant perturbations into the closed

loop algorithm, which will reduce its accuracy and might altogether prevent its convergence. Therefore, continuous tracking should be included whenever a closed loop system is used.

The test system was implemented using a very general and flexible model of speed controller. The cost estimate for this speed control subsystem in a 100 m^2 heliostat is \$60/m^2 when manufactured in a small series. This is expensive when considering the cost target of \$100–150/m^2 for the entire heliostat in commercial large-scale plants. However, it is possible to develop a simplified version of the controller, tailored only to the capabilities needed for heliostat control. This version can be significantly less expensive, especially when manufactured in large quantities, possibly down to \$20–30/m^2 for a 100 m^2 heliostat. The speed controller replaces other control elements in the existing design of a HC, which typically contribute about 10% of the overall heliostat cost [14]. The added cost due to the modification can therefore be about \$5–20/m^2. This could be a reasonable cost in our opinion, if the actual improvement in performance is significant enough. Detailed design and analysis are needed in order to validate these estimates.

Other implementations of continuous tracking are possible, for example using stepper motors. If a new heliostat is being designed from the ground up, then there is no need to retain traditional design practices, and alternative solutions can be considered. The selection of the appropriate solution would then depend on the heliostat size, the scale of production, the availability of advanced control electronics, etc.

The main conclusions from this work are:

- Continuous tracking can practically eliminate the tracking errors that are due to aim-point drift during step tracking intervals.
- Continuous tracking can increase the collection efficiency in high-performance heliostat fields.
- Continuous tracking can provide additional benefits such as reduced motor heating, reduced mechanical load on the heliostat structure and drive mechanism, and compatibility with accurate closed-loop control.
- For large-scale production, much tighter integration of the hardware should be developed, reducing the setup costs to a competitive level.

Acknowledgments

Support for this work was provided by the Israel Ministry of National Infrastructure.

References

[1] Vant-Hull, L. L., Izygon, M., and Imhof, A., 1999, ''Optimization of Central Receiver Fields to Interface with Applications Requiring High Flux Density Receivers,'' 9 Intl. Symp. Solar Thermal Concentrating Technologies, Journal de Physique IV, Flamant, G., Ferriere, A. and Pharabod, F., Eds., Font-Romeu, France, pp. 65–70.

[2] Buck, R., Bräuning, T., Denk, T., Pfänder, M., Schwarzbözl, P., and Tellez, F., 2001, ''Solar Hybrid Gas Turbine Based Power Tower Systems (REFOS),'' Solar Engineering 2001, Washington, D.C.

[3] Karni, J., Kribus, A., Rubin, R., Sagie, D., Doron, P., and Fiterman, A., 1997, ''The DIAPR: A High-pressure, High-temperature Solar Receiver,'' J. Sol. Energy Eng., **119**, pp. 74–78.

[4] Levy, I., and Epstein, M., 1998, ''Design and Operation of a High-power Secondary Concentrator,'' 9th International Symposium on Solar Thermal Concentrating Technologies, Flamant, G., Ferriere, A. and Pharabod, F., Eds., Odeillo, EDP Sciences, pp. 575–580.

[5] Monterreal, G., Garcia, G., Romero, M., and Barrera, G., 1997, ''Development and Testing of a 100 m2 Glass-metal Heliostat with a New Local Control System,'' Solar Engineering 1997, Washington D.C., pp. 251–259.

[6] Stone, K. W., and Lopez, C. W., 1995, ''Evaluation of the Solar One Track Alignment Methodology,'' Solar Engineering 1995, Lahaina (Hawaii), 1, pp. 521–526.

[7] Stone, K. W., and Sutherland, J. P., 1997, ''Solar Two Heliostat Tracking Performance,'' Solar Engineering 1997, Washington, D.C., ASME, pp. 237–242.

[8] Kribus, A., Vishnevetsky, I., and Yogev, A., 2002, ''Closed Loop Control of Heliostat Fields,'' 11th International Symp. Concentrating Solar Power and Chemical Energy Technologies, Zurich.

[9] Schubnell, M., and Ries, H., 1990, ''Velocity Controlled Tracking of the Sun,'' Solar Energy Materials 21, pp. 207–212.

[10] Duffie, J. A., and Beckman, W. A., 1991, ''Solar Engineering of Thermal Processes,'' Wiley, New York.

[11] Ries, H., Kribus, A., and Karni, J., 1995, ''Non-isothermal Receivers,'' J. Sol. Energy Eng., **117**, pp. 259–261.

[12] Kribus, A., Doron, P., Karni, J., Rubin, R., Reuven, R., Taragan, E., and Duchan, S., 2000, ''A Multistage Solar Receiver: The Route to High Temperature,'' Solar Energy 67, pp. 3–11.

[13] Kribus, A., Huleihil, M., Timinger, A., and Ben-Mair, R., 2000, ''Performance of a Rectangular Secondary Concentrator with an Asymmetric Heliostat Field,'' Solar Energy 69, pp. 139–151.

[14] Mancini, T., 2000, ''Catalog of Solar Heliostats,'' IEA SolarPACES Report III-1/00.